

Microfluidic Size Exclusion Chromatography (μ SEC) for Extracellular Vesicles and Plasma Protein Separation

Sheng Yuan Leong, Hong Boon Ong, Hui Min Tay, Fang Kong, Megha Upadya, Lingyan Gong, Ming Dao, Rinkoo Dalan, and Han Wei Hou*

Extracellular vesicles (EVs) are recognized as next generation diagnostic biomarkers due to their disease-specific biomolecular cargoes and importance in cell–cell communications. A major bottleneck in EV sample preparation is the inefficient and laborious isolation of nanoscale EVs (\approx 50–200 nm) from endogenous proteins in biological samples. Herein, a unique microfluidic platform is reported for EV-protein fractionation based on the principle of size exclusion chromatography (SEC). Using a novel rapid (\approx 20 min) replica molding technique, a fritless microfluidic SEC device (μ SEC) is fabricated using thiol-ene polymer (UV glue NOA81, Young's modulus \approx 1 GPa) for high pressure (up to 6 bar) sample processing. Controlled on-chip nanoliter sample plug injection (600 nL) using a modified T-junction injector is first demonstrated with rapid flow switching response time ($<$ 1.5 s). Device performance is validated using fluorescent nanoparticles (50 nm), albumin, and breast cancer cells (MCF-7)-derived EVs. As a proof-of-concept for clinical applications, EVs are directly isolated from undiluted human platelet-poor plasma using μ SEC and show distinct elution profiles between EVs and proteins based on nanoparticle particle analysis (NTA), Western blot and flow cytometry analysis. Overall, the optically transparent μ SEC can be readily automated and integrated with EV detection assays for EVs manufacturing and clinical diagnostics.

1. Introduction

Extracellular vesicles (EVs) are cell-derived nanoscale (50 to 200 nm) phospholipid bilayer vesicles^[1] which are important for intercellular communication.^[2] The EV-based cargoes (DNA, RNA, lipids, proteins), indicative of cell origin and disease status, have also emerged as potential next generation

biomarkers in cancers and metabolic diseases.^[3–6] Due to their abundance in body fluids and easy uptake by recipient cells,^[7] many EV-based diagnostic^[8] and therapeutic^[9–11] applications have received increasing attention in recent years.

Size exclusion chromatography (SEC) is widely used for clinical EVs isolation^[12] as it is simple to operate, and produces EVs with higher yield and lower protein contamination as compared to ultracentrifugation (UC).^[13–15] As SEC is performed using commercial prepacked SEC columns^[16] or self-packed columns with Sepharose beads,^[17] integrating with upstream sample preprocessing and downstream analysis remain challenging due to sample batch processing mode and column design.

Microfluidics is an enabling technology which have been used to directly isolate EVs from complex biofluids such as blood.^[18–21] Miniaturization of chromatography systems offers several advantages including reduced reagent consumption, lower cost, and faster analysis with increased detection sensitivity.^[18,19,22]

Recent advances in microfluidic chromatography have reported on-chip integration with UV detector,^[23] LED detector,^[24,25] and mass spectrometer.^[26] However, these devices mostly focus on isolation of smaller biomolecules such as proteins, lipids, and drug molecules^[27] while larger EVs remains largely unexplored. Two major technical challenges faced in miniaturized SEC are on-chip sample injection and chip material suitable

S. Y. Leong, H. B. Ong, H. M. Tay, L. Gong, H. W. Hou
School of Mechanical and Aerospace Engineering
Nanyang Technological University
50 Nanyang Avenue, Singapore 639798, Singapore
E-mail: hwhou@ntu.edu.sg

F. Kong, M. Upadya, M. Dao
School of Biological Sciences
Nanyang Technological University
60 Nanyang Drive, Singapore 637551, Singapore

 The ORCID identification number(s) for the author(s) of this article can be found under <https://doi.org/10.1002/sml.202104470>.

DOI: 10.1002/sml.202104470

M. Dao
Department of Material Science and Engineering
Massachusetts Institute of Technology
77 Massachusetts Avenue, Cambridge, MA 02139, USA

R. Dalan
Endocrine and Diabetes
Tan Tock Seng Hospital
11 Jalan Tan Tock Seng, Singapore 308433, Singapore

R. Dalan, H. W. Hou
Lee Kong Chian School of Medicine
Nanyang Technological University
11 Mandalay Road, Clinical Sciences Building, Singapore 308232, Singapore

for high pressure flow operation. Successful miniaturization of commercial rotary valve injector^[28,29] and microfluidic passive injector using cross junction^[30–32] or T-junction^[33] channel designs have been reported. However, the former method requires costly valve components, while the latter on-chip flow modules are sensitive to small pressure changes at low flow rates. Polydimethylsiloxane (PDMS), a common material for microfluidic devices, is not suitable for high pressure SEC operations due to substantial channel deformation with its low Youngs' modulus (0.8–2.5 MPa).^[34–36] Thermoplastics polymers such as cyclic olefin polymers (COC)^[37] and poly(methyl methacrylate) (PMMA)^[38] have better mechanical properties (Youngs' modulus \approx 3 GPa), but their low feature resolution ($>$ 50 μ m) requires integration of external frit which complicates the fabrication process. Photocurable thiol-ene polymer is an attractive alternative with high feature resolution down to 20 μ m, high Youngs' modulus (\approx 1 GPa), bonding strength, chemical stability and good optical transparency.^[39,40] However, it is difficult to fabricate fritless thiol-ene SEC columns due to the broad range of channel dimension ranging from tens of micron (for micropillars) to several millimeters (for resin column).

Herein, we report a novel fritless microfluidic SEC device (μ SEC) using thiol-ene polymer (UV glue NOA81) for EVs isolation and protein separation. Using a simple three-step replica molding, a multi-height (20 to 280 μ m) SEC microchannel was fabricated without the need for high pressure/temperature, and the device was subsequently packed with commercial SEC resin. We first demonstrated on-chip nanoliter sample plug injection using a modified T-junction design by regulating hydraulic resistances to enable fast ($<$ 1.5 s) sample injection. We further validated the μ SEC using fluorescence nanoparticles (50 nm), albumin and breast cancer cells (MCF-7) derived EVs to study the retention time and separation resolution. Finally, we applied the device to isolate EVs from human platelet poor plasma (PPP), and showed comparable EV concentration and purity as commercial SEC columns based on nanoparticle particle analysis (NTA), Western blot and flow cytometry analysis. Taken together, the developed low cost μ SEC can be readily integrated with upstream microfluidic sample preparations and downstream EV detection assays to create automated and portable solutions for EVs manufacturing or clinical EV-based diagnostics.

2. Results

2.1. EVs Isolation Using Miniaturized SEC Device (μ SEC)

Figure 1 illustrates the setup of the μ SEC system. The multi-height microfluidic device has two inlets, three outlets at inlet/outlet region with 20 μ m height (highlighted in blue), and one inlet at packing region with 280 μ m height (highlighted in red and grey) (Figure 1A and Figure S1: Supporting Information). The inlet region consists of three T-junctions, with the 1st T-junction connecting to sample flow and outlet 1; 2nd T-junction connecting to sheath flow and three-way valve; and 3rd T-junction joining 1st and 2nd T-junctions. The other two ends of three-way valve are connected to outlet 2 and outlet 3 separately. Two PDMS channels with 20 μ m height are connected to outlet 1 and 2 in series to increase their hydraulic resistance

(Figure S1B, Supporting Information). Both continuous sample and sheath flow are driven by separate syringe pumps. Micropillars of 20 μ m diameter located on both ends of resin packing region (red region) act as filters to avoid resin leakages during packing (Figure S1C, Supporting Information). Commercial SEC resin (qEV, IZON) with bead diameter between 25 to 75 μ m is packed into μ SEC by injecting into the top inlet of packing region followed by UV glue sealing (Figure 1B). As PDMS has lower fluorescent background compared to UV glue,^[41] a PDMS detection channel (400 μ m width) is connected downstream to μ SEC device to enable fluorescence detection (Figure S1D, Supporting Information).^[41] During device operation, a sample plug (consisting of EVs and proteins) is generated by the T-junction under continuous sample and sheath flow, which will enter the SEC channel. EVs with larger hydrodynamic diameter ranging between 50 nm to 1 μ m are excluded by the pores of SEC resin, while proteins with smaller hydrodynamic diameters ($<$ 30 nm) diffuse into the resin pores which results in slower elution speed as compared to EVs (Figure 1C). EVs are therefore eluted as earlier fractions to achieve protein separation.

2.2. Rapid Prototyping of μ SEC Using UV Glue

Figure 2 illustrates the fabrication process of μ SEC device through a three-step replica molding. Unlike PDMS, UV glue is not compatible with SU-8 mold as it tends to fill up tiny roughness holes on the mold surface after curing.^[39] Curing of UV glue is partially inhibited in the presence of oxygen, leaving a semi-cure surface which facilitates demolding.^[42] Therefore, a gas permeable PDMS mold was used as an alternative master mold for replica molding of UV glue. A PDMS negative mold was first fabricated from SU-8 master mold and holes were punched at inlet/outlet region (Figure 2A). This created extruded pillar structures after second PDMS replica molding and intruded holes at the inlet/outlet region in the third UV glue replica molding (Figure 2B,C). Compared to post curing hole punching or using metal insert on master mold to create extruded pillar structures, the proposed method can minimize surface deformation and stresses induced during post curing hole punching or withdrawal of metal insert, which increases the bonding strength between two UV glue surfaces. A thin film of UV glue was drop cast onto glass slide to act as interfacing adhesive between glass slide and μ SEC channel (Figure 2D).^[43] The bonding was further strengthened by plasma treating both UV glue channel and thin film before bonding.

2.3. Sample Plug Generation Using a Modified Three T-Junction Injector

We adopted an on-chip passive sample injection method to avoid complicated valve components and excessive dead volumes in the connectors and tubings. In microfluidic devices with operating flow rates in nL to μ L min⁻¹ range, pressure propagation from syringe pump to injector is slow, resulting in lagging response of flow switching between sample and sheath flow. Hence, conventional three T-junction injector^[33] is sensitive to slight pressure changes, tubing movements, pump actuation

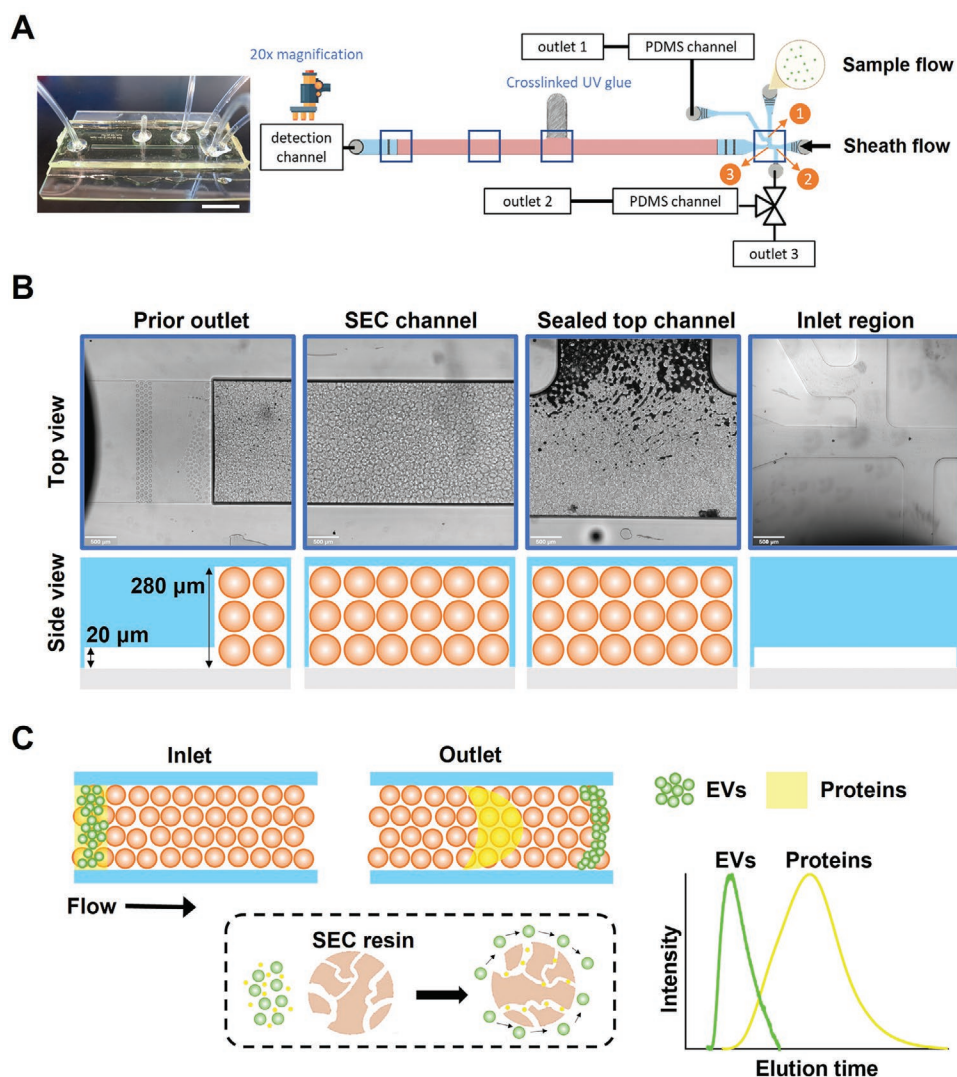


Figure 1. EVs isolation using miniaturized size exclusion chromatography (μ SEC). **A**) Photo and schematic design of μ SEC. Scale bar: 2 cm. On-chip sample injector consists of three T-junction injectors (T-junctions labeled as 1, 2, and 3) with varying outlet hydraulic resistance due to additional PDMS channels for outlet 1 and 2. A PDMS detection channel is connected at the μ SEC outlet for fluorescence imaging. **B**) Optical images of different channel regions indicated by blue boxes in (A) and corresponding channel cross sectional view packed with SEC resin (orange). Scale bar: 500 μ m. **C**) Schematic illustration of EVs isolation mechanism in μ SEC. Sample plug (EVs and proteins) flow is introduced into the μ SEC channel using a 3-way valve. EVs of larger sizes (50 nm to 1 μ m) are excluded by resin pores and elute out in earlier fractions while smaller proteins diffuse into the pores and elute later.

and sample viscosity, which deteriorates the consistency in plug injection volume. To address this problem, we improved the design by connecting additional PDMS microchannels to outlet 1 and 2, thus increasing the hydraulic resistance differences to achieve faster flow switching. A three-way valve was also used at bottom outlet of T junction (T junction 3, Figure 1C) instead of sample inlet to reduce sample dead volume in the valve. **Figure 3** illustrates the process of sample plug generation in μ SEC. At the initial state (step 1), the valve was set to high resistance outlet 2. Sheath flow (50 μ L min^{-1}) flowed into center channel and outlet 2, while the sample flow (5 μ L min^{-1}) was diverted to outlet 1. At step 2, valve position was manually switched to low resistance outlet 3 to divert sheath flow into outlet 3 while introducing a short sample plug into center channel. When the valve position was switched back to the high resistance outlet 2

(step 3), sample flow was terminated as sheath flow would enter both outlet 1 and 2 to completely cut off sample flow. Injection volume can be derived based on fluorescent area of FITC-BSA plug (Figure 3B). The area estimated was 1.98812 mm^2 , which equates to an injection volume 0.5567 μ L in the center channel with 280 μ m height. This design demonstrated a versatile and fast nanoliter (<1.5 s in Figure 3B) sample plug injection using a simple continuous flow setup with two syringe pumps and a manual three-way valve.

2.4. Characterization of μ SEC Separation Performance

To study EVs separation in the μ SEC, we first characterized the elution profiles of fluorescent 50 nm beads and FITC-BSA

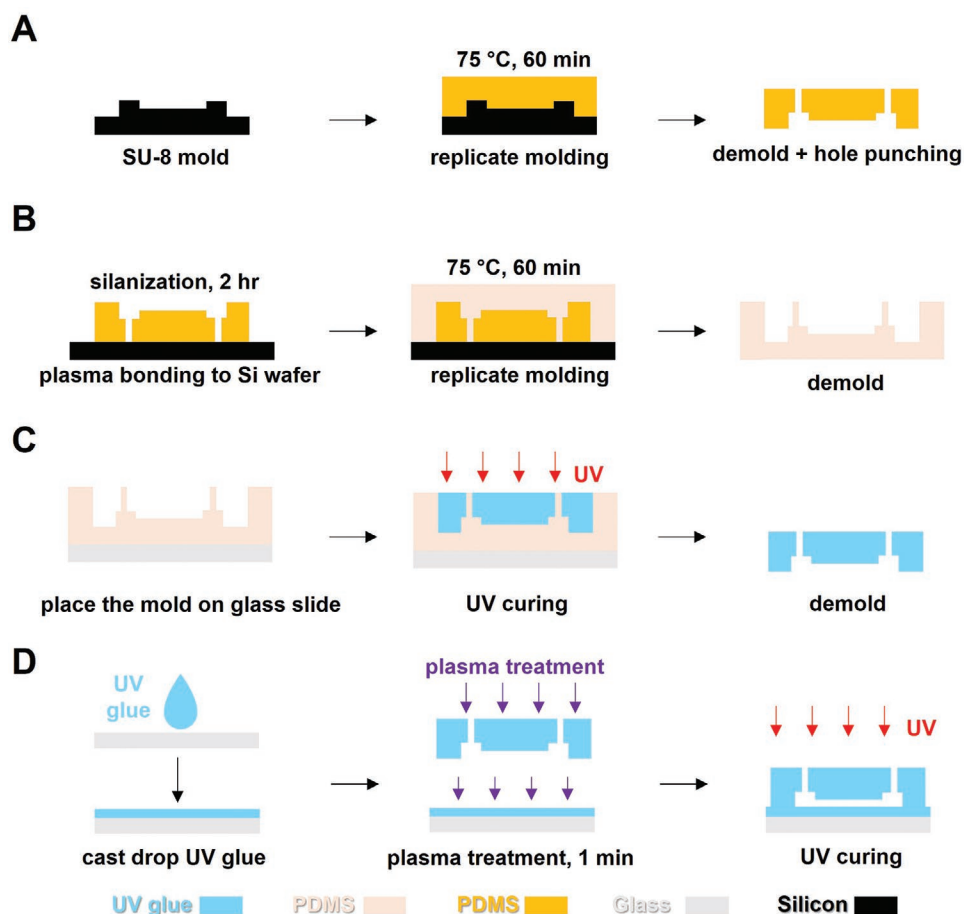


Figure 2. Fabrication of μ SEC using UV glue. A) Fabrication of negative PDMS mold with inlet holes. B) Fabrication of positive PDMS mold with inlet pillars. C) Replica molding of μ SEC channel using UV glue. D) Drop casting of UV glue on glass side and bonding of μ SEC.

which represent EVs and plasma albumin, respectively. Fluorescent intensity of each sample was normalized to its maximum intensity. Representative chromatograms at different flow rates from 1.77 to 5.46 $\mu\text{L min}^{-1}$ (of center channel) showed distinct 50 nm and FITC-BSA peaks at different timepoints, clearly indicating the ability of the device to separate 50 nm beads from FITC-BSA (Figure 4A). We next quantified, two parameters namely the retention time and resolution to assess the separation performance of μ SEC. Retention time is defined as the time difference between injection time and maximum intensity peak, while resolution is defined as the retention time difference between 50 nm beads and FITC-BSA divided by average base width of these two peaks (Figure 4B). The base width was set at 10% of normalized maximum intensity to reduce fluorescence background noise created by non-specific sticking of fluorescent beads and BSA in the PDMS detection channel. Both resolution and retention time difference between two peaks exhibited decreasing trend with increasing flow rate, with highest magnitudes observed at center channel flow rate less than 2 $\mu\text{L min}^{-1}$. This suggests that the diffusion process of FITC-BSA was reduced at higher flow rates possibly due to stronger convection, which led to narrower retention time differences between 50 nm beads and FITC-BSA (Figure 4C,D). Elution time of 50 nm beads increased three times from

350 s at 5.46 $\mu\text{L min}^{-1}$ to 1050 s at 1.77 $\mu\text{L min}^{-1}$, while resolution increased from 0.65 to 1.05. Hence the operating flow rate of $1.5 \pm 0.25 \mu\text{L min}^{-1}$ was set for subsequent studies. We further characterized the exclusion limit of μ SEC device using fluorescent 500, 100, 50 nm beads and FITC-BSA. Similar bead elution profile (50 to 500 nm) was observed with elution peak between 640–700 s followed by a distinct FITC-BSA peak at 1450 s. This result indicated that the beads were mostly excluded by resin pores and eluted earlier than FITC-BSA which was dominated by diffusion (Figure 4E). We also observed a slight delay in elution peak of 100 and 50 nm beads (≈ 690 s) as compared to 500 nm beads (≈ 640 s), which suggests some limited diffusion of 100 and 50 nm beads into the resin pores with a size cut-off of ≈ 70 –75 nm (Figure 4F). Taken together, our results showed that the μ SEC device is capable of separating 50–500 nm beads (similar size range as EVs (≈ 40 –200 nm)) from FITC-BSA (mimicking plasma proteins) based on different elution time.

2.5. μ SEC Characterization Using Cancer Cells (MCF-7) Derived EVs

After beads validation, EVs isolated (by ultracentrifugation) from breast cancer cell MCF-7 culture medium were stained with PKH67 dye and injected into μ SEC to determine the effect

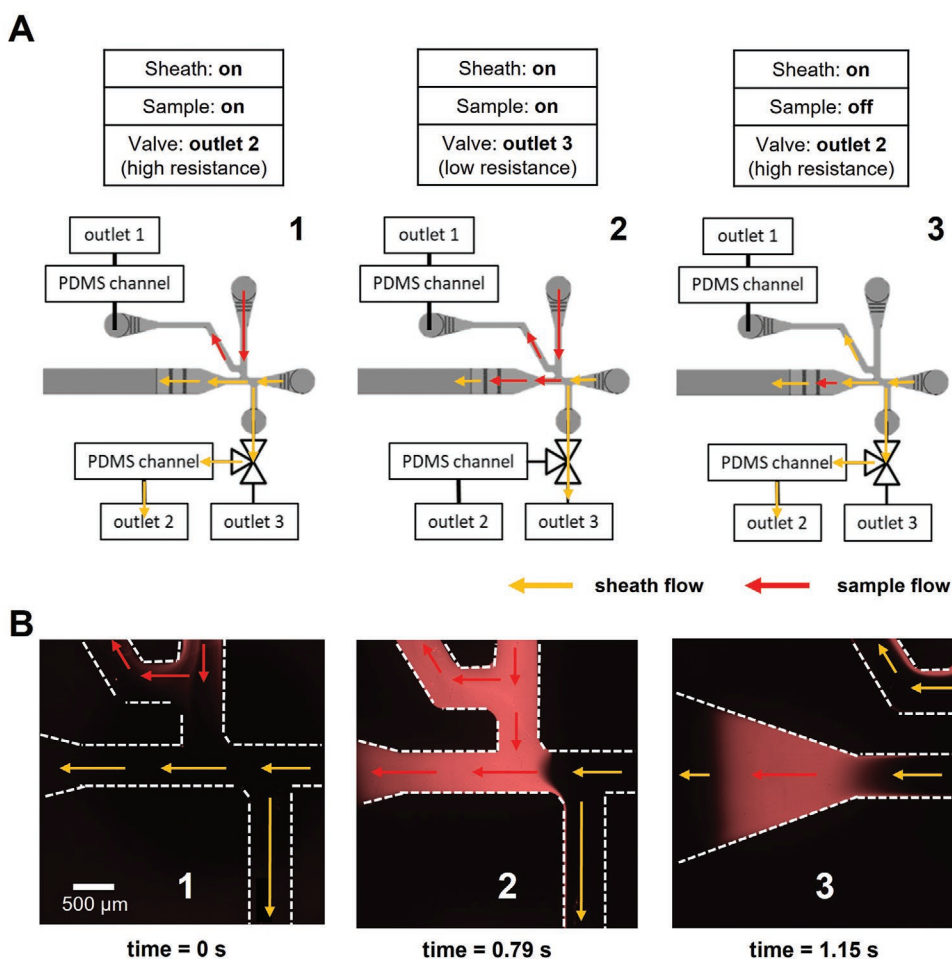


Figure 3. Sample plug flow generation using a modified three T-junction injector. A) Coordination of sample pump, sheath pump and a 3-way valve during plug flow generation. In step 1, sample flow was directed into outlet 1 by higher flow rate of sheath flow into the center channel. In step 2, sheath flow entered outlet 3 of lower resistance by valve switching, which allowed diversion of sample flow into the center channel. In step 3, sample flow was stopped as the valve was switched back to outlet 2. Sheath flow would enter the center channel to cut off sample injection and form a sample plug flow. B) Fluorescent images of FITC-BSA's plug generation corresponding to Figure 3A.

of injection volume on separation performance. As PKH dye is prone to micelles formation in saline buffer,^[44–47] particle concentrations in UC pellets derived from MCF-7 culture medium (indicative of EVs & micelles) and blank cell culture medium (indicative of micelles) after PKH67 staining were compared using nanoparticle tracking analysis (NTA) (Figure S2, Supporting Information). Based on NTA results (limit of detection (LoD) ≈ 80 nm) using both scatter and fluorescent detection modes, we estimated that $\approx 20\%$ of particles detected in PKH67-stained MCF-7 EVs were micelles (staining artefacts). It should be noted that this will likely be an underestimate due to unclear micelles abundance below LoD of NTA. Presence of these small PKH67+ EVs/micelles would result in an EV elution profile with longer tail but should not affect the overall size exclusion effects of EVs/particles (≈ 80 to 200 nm) in μ SEC at earlier elution timepoints. Consistent with the bead results, a clear separation between MCF-7 EVs and FITC-BSA (fixed injection duration of 30 s) was observed for both EVs injection duration of 15 and 30 s (Figure 5A,B). Both conditions produced comparable EV retention time (≈ 760 s vs ≈ 820 s), with longer tail

extending to 1500 s for 30 s injection duration as compared to 1160 s in 15 s injection duration.

Elution of FITC-BSA occurred at 1200 to 3000 s (peak at 1960 s) and had minimal differences in retention time (1200 s (15 s injection) versus 1140 s (30 s injection)). In Figure 5C, EVs located at channel centre (higher flow velocity due to parabolic flow profile) first appeared in the channel middle at 800 s, followed by EVs closer to channel wall (with lower flow velocities) which corresponded to the second smaller peak at 1160 s. It should be noted that due to increased EVs size after staining and repetitive UC, few larger EVs with stronger fluorescent signal were observed and contributed to the longer tail between 1300 and 1500 s.

2.6. EVs Isolation from Human Plasma Using μ SEC

As a proof-of-concept for clinical testing, we isolated EVs from undiluted human platelet-poor plasma (PPP) using μ SEC and commercial SEC column (cSEC, qEVsingle from IZON)

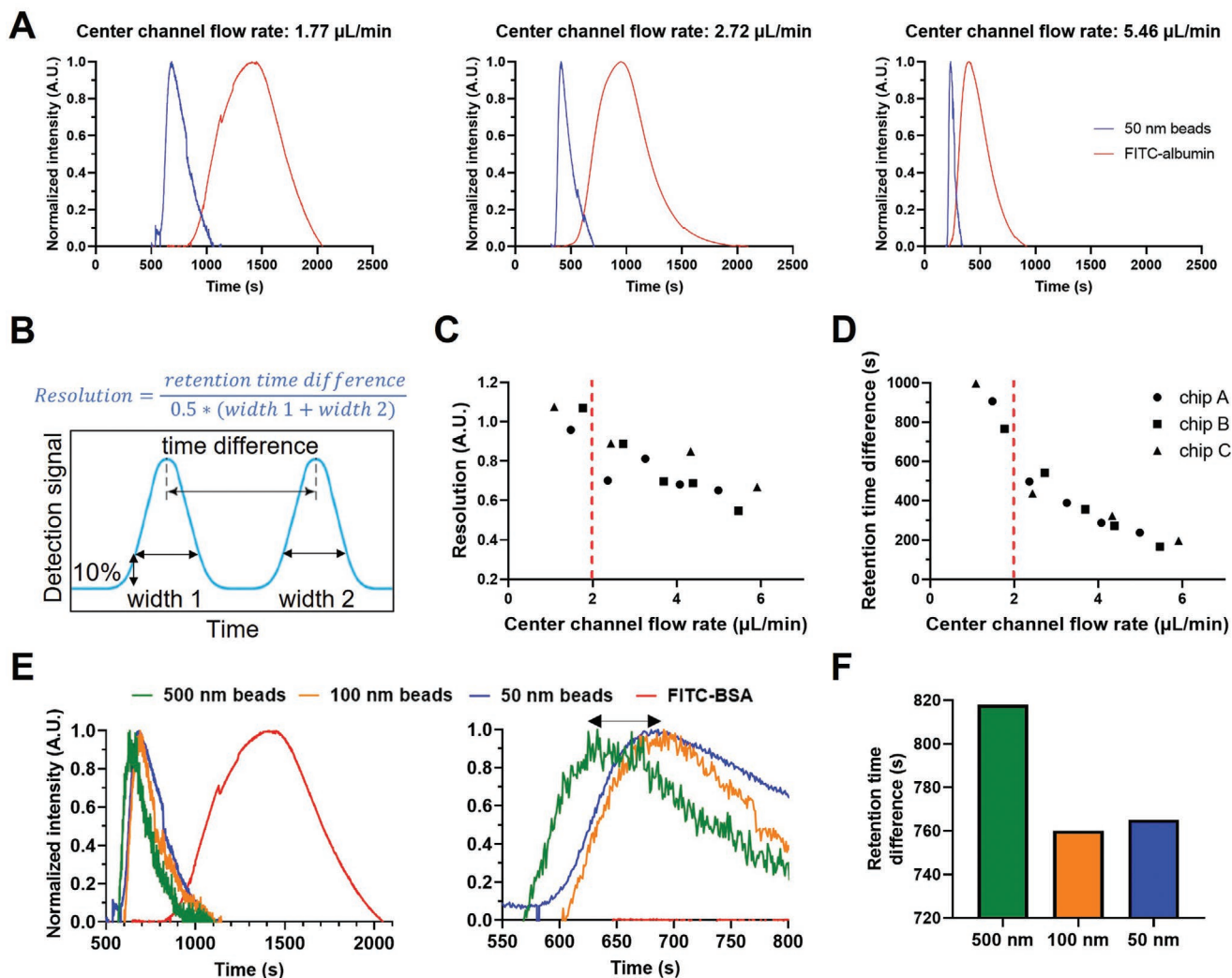


Figure 4. Characterization of μ SEC separation performance. A) Chromatogram of 50 nm polystyrene beads and FITC-albumin at different center channel flow rate. B) Performance metric of SEC. C) Separation resolution (based on 10% peak height) and D) retention time difference at different center channel flow rates. Highest resolution and retention time difference were observed at center channel flow rate $< 2 \mu\text{L min}^{-1}$. E) Chromatogram of 50, 100, and 500 nm beads and FITC-BSA at center channel flow rate of $1.74 \mu\text{L min}^{-1}$ (left). Magnified view indicates peak shift of 500 nm bead elution (right). F) Retention time differences of different bead sizes.

(Figure 6A). Different centrifugation methods (1-spin, 3-spin, 3-spin + $0.45 \mu\text{m}$ filter, 4-spin, 4-spin + $0.45 \mu\text{m}$ filter) were first compared to study depletion of platelets ($\approx 2\text{--}3 \mu\text{m}$) and platelet fragments ($\approx 500\text{--}1000 \text{ nm}$) (Figure S3A, Supporting Information). Flow cytometry analysis (minimum detectable size of 500 nm based on in-house testing) based on CD41a+ expression showed negligible platelet count in both 3-spin and 4-spin methods, and lowest platelet fragment count in 4-spin + filter method, thus indicating efficient platelets removal from plasma (Figures S3B and S4A: Supporting Information). There were also negligible changes in particle concentration (based on NTA) before and after filtration of PPP obtained using the 4-spin method (Figure S4B,C: Supporting Information). Hence the optimal PPP isolation protocol (4-spin + filter) was used for subsequent studies. Sample plug injection was increased to 60 s to generate sufficient eluent volume and concentration for nanoparticle tracking analysis.

Elution of particles in μ SEC started from 900 s and peaked at 1100 s, while elution of proteins (measured by bicinchoninic acid assay, BCA) occurred from 1300 s and peaked at 1900 s (Figure 6B). Similar elution profile was observed in cSEC, in which particles elution started from fraction 6 and peaked at fraction 8, followed by proteins elution starting from fraction 12 and peaked at fraction 17 (Figure 6C). Comparison between μ SEC and cSEC using PPP from same donors also showed similar particle and protein concentrations in both methods (Figure S5, Supporting Information), which suggests that the observed standard deviations may be attributed to patient-to-patient variations in their plasma content. While particles detected by NTA may include non-EV particles (e.g., lipoproteins), both EVs and non-EV particles would likely be excluded by the resin pores together due to their similar size. Fractions with highest particle concentration (900–1300 s in μ SEC and fraction 7–9 in cSEC) were then pooled as

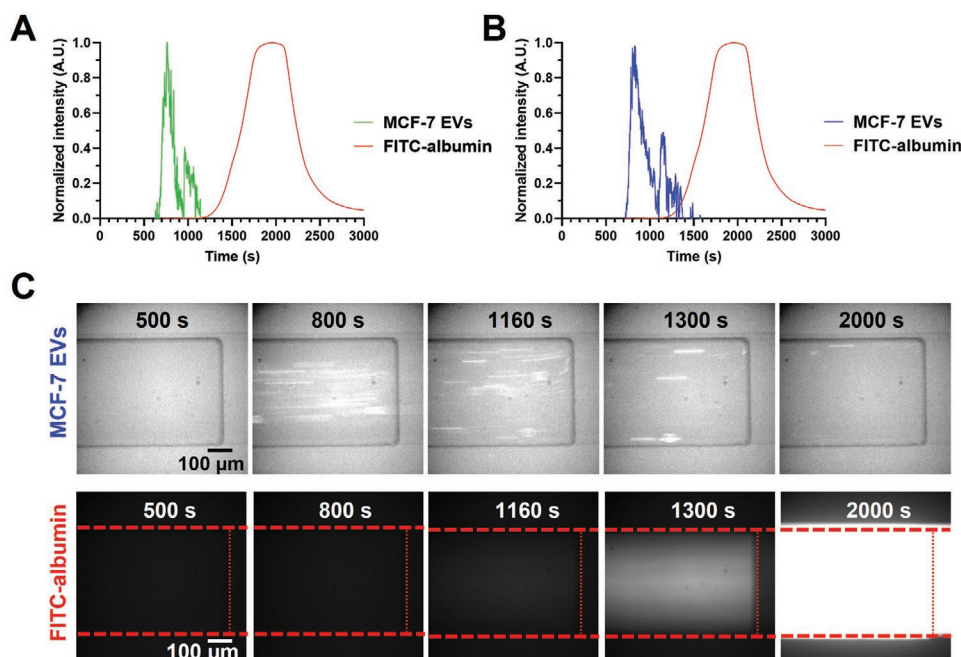


Figure 5. μ SEC characterization using cancer cells (MCF-7) derived EVs. Average fluorescent intensity during elution of MCF-7 EVs and FITC-albumin for A) 15 s and B) 30 s sample injection duration. Center channel flow rate: $1.51 \mu\text{L min}^{-1}$. C) Corresponding fluorescent images of MCF-7 EVs and FITC-albumin in the PDMS detection channel at different time points.

EV fractions for downstream characterization. NTA indicated particle size of less than 200 nm in μ SEC and cSEC EV fractions (Figure 6D,E). TEM images showed EVs surrounded by lipoproteins (Figure 6F), and the presence of EVs and lipoproteins were further confirmed by positive EV markers (Flotillin-1, CD81) and lipoprotein markers (ApoA, ApoB) based on Western blot analysis (Figure 6G). It should be noted that protein contamination was greatly reduced in μ SEC EV fractions based on smaller albumin bands and BCA result, which indicates efficient separation of EVs and plasma proteins. Due to $\approx 40\%$ shorter column length in μ SEC as compared to cSEC, some albumin remained present in the EV fractions of μ SEC, which can be further improved with longer SEC channel. The retention time difference of μ SEC was ≈ 800 s, and earlier protein elution (≈ 1300 s) was observed in plasma sample compared to FITC-BSA (≈ 1500 s, ≈ 66 kDa) possibly due to presence of larger plasma proteins such as IgG (≈ 150 kDa) and IgM (≈ 970 kDa). Finally, we performed flow cytometry analysis of EV-bound aldehyde beads and observed comparable EV markers expression (CD9 and CD81) for both μ SEC and cSEC (Figure 6H). Taken together, these results clearly demonstrated that the developed μ SEC can isolate EVs from undiluted plasma samples with similar separation performance as cSEC, which can be further developed for clinical diagnostics.

3. Discussion

In this work, we have developed a novel fabrication method for high pressure fritless microfluidic SEC device (μ SEC) using commercial thiol-ene polymer (UV glue NOA 81). Due to short curing time of UV glue, the replica molding process

is significantly shortened from hours to ≈ 20 min compared to PDMS replica molding ($\approx 1\text{--}2$ h). μ SEC device can be easily fabricated using low-cost UV light source (< 30 US dollar) unlike the more expensive hot pressing in COC and PMMA bonding processes. UV glue properties also possess a good balance between feature resolution ($20 \mu\text{m}$) and Young's modulus (≈ 1 GPa),^[48] which enables fabrication of micropillars with $20 \mu\text{m}$ diameter as built-in frit and avoid the need of additional membrane components. With semi-curing of UV glue and flexible extruded pillar at inlet/outlet region on PDMS mold, built-in inlet/outlet holes can be created without affecting surface flatness during demolding. This is critical for subsequent bonding between two hard surfaces of μ SEC channel and glass slide. Built-in inlet/outlet connector ports also allow direct tubing connection to μ SEC device, eliminating band dispersion due to dead volume in connectors and tubings. Lastly, UV glue provides fast and strong sealing for column packing and tubing connection due to similar chemistry between UV glue and μ SEC device. Taken together, this fabrication technique provides more flexibility in designing microfluidic devices for high-pressure applications such as miniaturized liquid chromatography^[22,26,27] and microfluidic sample injector for mass spectrometry.^[40]

We also report a novel design for robust and rapid (< 1.5 s) nanolitre sample injection using a modified three T-junction injector. By increasing hydraulic resistance differences among different injector outlets, fluid paths of sample and sheath flow become more stable which reduce the risks of sample leakage into center channel due to pressure imbalance or lagging pressure propagation from syringe pumps. Besides, ≈ 600 nL of sample plug injection can be achieved using syringe pumps operating at $\mu\text{L min}^{-1}$ range. The addition of a three-way valve at downstream of T-junction injector also ensures minimal

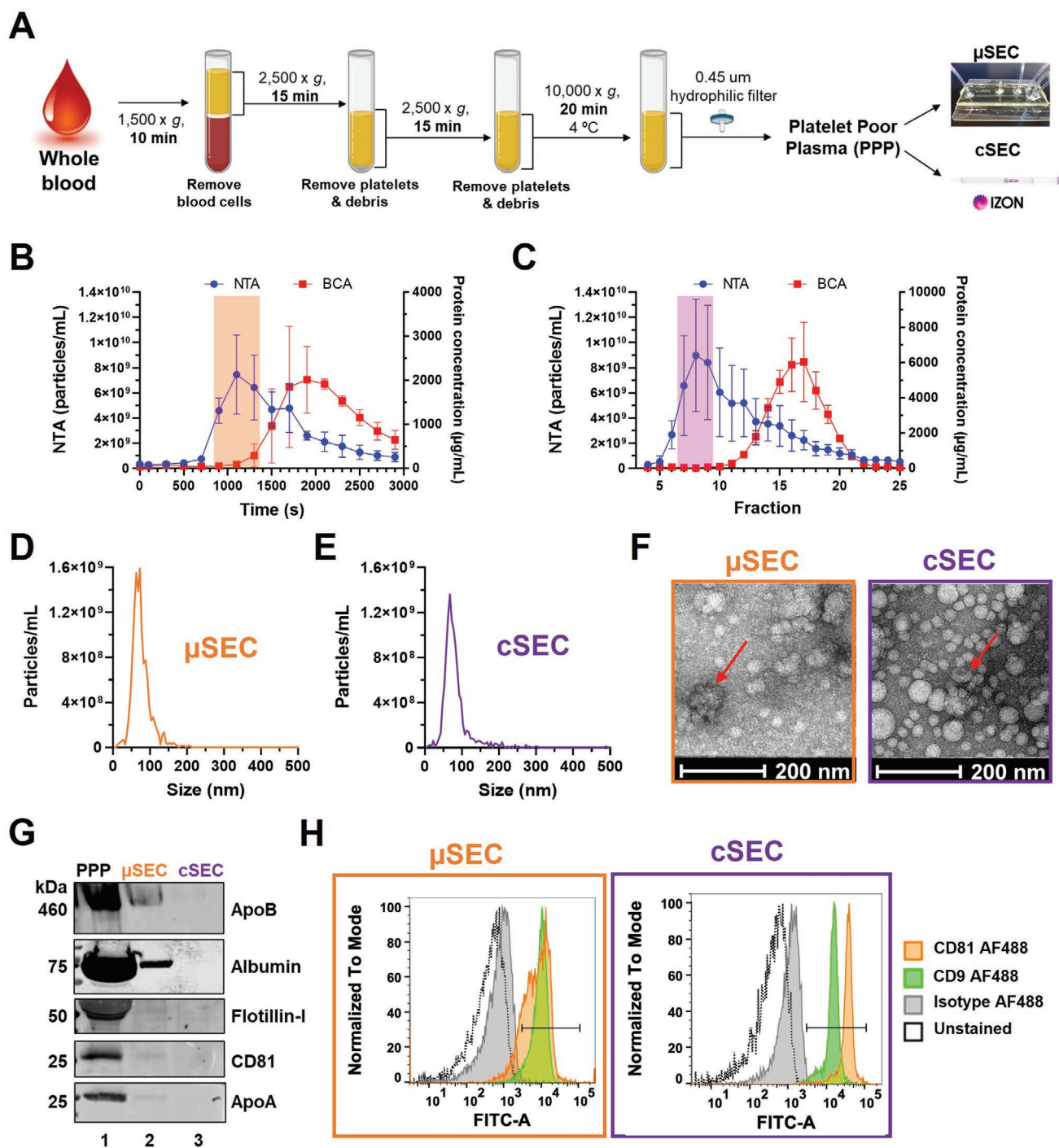


Figure 6. EVs isolation from human plasma. A) Workflow of EVs isolation from human plasma using μ SEC device and commercial SEC column (cSEC, qEVsingle from IZON). Average particle concentration (NTA) and protein concentration (BCA) of different eluted fractions for B) μ SEC ($n = 4$) and C) cSEC ($n = 3$). EV eluent fractions are highlighted in orange (fraction 900–1300 s) for μ SEC and purple (fraction 7–9) for cSEC, respectively. Representative particle size distribution of EV fractions for D) μ SEC and E) cSEC. F) Transmission electron microscopy images of μ SEC and cSEC fractions. EVs are indicated by red arrow. G) Western blot indicating EV markers (Flotillin-1, CD81), lipoprotein markers (ApoB, ApoA) and plasma protein (Albumin) in PPP, μ SEC EVs and cSEC EVs. μ SEC and cSEC EVs were loaded with equal volume (22 μ L) except plasma (0.5 μ L). H) Flow cytometry analysis of CD9 and CD81 expression on EV-bound aldehyde microbeads from μ SEC and cSEC EV fractions. Data were presented as mean \pm s.d.

sample dead volume in the valve. We estimated a dead volume of ≈ 200 nL between T junction injector and SEC packing region, which is ≈ 10 times smaller compared to dead volume of

typical fluidics tubing (≈ 2 μ L in 1 cm long 0.02" ID tubing). It should be noted that despite the post column dispersion in the connecting tubings, two distinct peaks of PKH67-stained EVs

and FITC-BSA were still observed, which indicates negligible disturbance to the EVs separation. We also demonstrated comparable EV separation performance with human plasma samples between μ SEC (42% shorter column length) and cSEC.

In this work, the developed μ SEC reduces sample volume in cSEC from ≈ 100 to ≈ 5 μ L, and EV elution volume from ≈ 600 to ≈ 10 μ L. We envision that the μ SEC platform would be beneficial for single EV analysis,^[49] real-time EV detection or screening applications (e.g., EV cargo loading) that require low EV sample volumes but have many experimental conditions. With its modular design and continuous-flow processing, the μ SEC device can be automated and enables easy coupling with other microfluidic EV isolation^[20] or EV-based assays^[50,51] to develop complete “sample in-answer out” EV profiling or diagnostics solutions. As future work, EV detection modules can be directly integrated into μ SEC device after post column micro-pillar region to reduce post column dispersion and shorten elution time. With the current chip dimensions (5 cm (length) \times 2 mm (width) \times 280 μ m (height)), throughput of μ SEC can be further increased by scaling up column dimensions or device multiplexing.

4. Conclusion

In summary, we have developed a novel fritless microfluidic size exclusion chromatography (μ SEC) for integrated EVs isolation and on chip monitoring using commercial off-the-shelf UV glue. High feature resolution (20 μ m) and Young's modulus (≈ 1 GPa) of UV glue allows fabrication of micropillars as built-in frit to minimize band broadening effect due to dead volume within injector. Our device offers key advantages such as a) simple and rapid fabrication process using a three-step replica molding, and b) modular design for direct coupling with upstream/downstream modules. We also demonstrated rapid (< 1.5 s) generation of nanolitre sample plug injection using a modified passive T junction injector which improved flow switching response time and pressure stability. We envision that the current μ SEC system with simple setup of two syringe pumps can be readily automated and integrated with downstream EV detection or assays for real time monitoring tool in EVs manufacturing or EV-based clinical applications.

5. Experimental Section

EVs Staining: Three T75 flasks of MCF-7 cells were cultured in serum-free medium supplemented with 10% fetal bovine serum (Cytiva HyClone Fetal Bovine Serum, South American Origin, Cytiva Inc., Marlborough, MA, USA) and 1% penicillin-streptomycin (HyClone Penicillin-Streptomycin, Cytiva Inc., Marlborough, MA, USA) and maintained at 37 °C in a humidified 5% CO₂ incubator. After confluency, the cells were supplied with 10 mL of serum-free medium at 70% confluency and grown for another 48 h for EVs secretion into the medium. The conditioned medium was harvested and centrifuged at 300 \times g for 10 min, then 2000 \times g for 20 min to remove floating cells and debris. The supernatant was passed through a 0.22 μ m syringe filter prior to UC at 210 000 \times g for 70 min at 4 °C to pellet the EVs. After supernatant was poured out, UC tube was inverted upside down and vacuumed using suction pump to remove supernatant remnant on UC tube. The EV pellet was stained

with PKH67 Green Fluorescent Cell Linker Kit (Sigma-Aldrich, St. Louis, MO, USA). It was then washed at 210 000 \times g for 70 min at 4 °C to remove unbound PKH67 dye and the pellet was resuspended in 100 μ L of PBS and kept at -20 °C for storage up to 2 months.

PDMS Mold Fabrication: 10:1 w/w ratio of polydimethylsiloxane (PDMS) with curing agent (SYLGARD 184 Silicone Elastomer Kit, Dow Corning Inc., Midland, MI, USA) was mixed and poured onto SU-8 mold before baking at 75 °C for 60 min to create a negative PDMS mold with reverse feature polarity. After demolding, holes were created at inlet/outlet regions using 1.5 mm biopsy puncher. The negative PDMS mold was cleaned thoroughly with isopropanol and dried at 75 °C for 15 min. The negative PDMS mold and a silicon wafer were then plasma treated (PDC-002, Harrick Plasma Inc., Ithaca, NY, USA) at high power setting for 1 min before bonding the non-featured side of PDMS to the silicon wafer to form the mold for second replicate molding. The negative PDMS mold was functionalized with silane (Trichloro(1H,1H,2H,2H-perfluorooctyl)silane, Sigma-Aldrich, St. Louis, MO, USA) in a vacuum chamber for 2 h. PDMS mixture was cast on the negative PDMS mold using same casting protocols above, and a positive PDMS mold with positive feature polarity and extruded pillars at inlet/outlet regions was created. A 50 mm \times 75 mm microscopy glass slide was plasma treated for 2 min and bonded to the non-featured side of positive PDMS mold to support the mold and prevent mold bending after curing of UV glue (NOA 81, Norland Products Inc., East Windsor, NJ, USA).

Fabrication of μ SEC Device: UV glue (NOA 81, Norland Products Inc., East Windsor, NJ, USA) was cast on positive PDMS mold and UV cured (36 W UV manicure machine, Yiwu Lidan Cosmetics Co., Ltd. Yiwu, Zhejiang, China). The cured UV glue channel was carefully demolded without bending the channel to maintain its surface flatness. To create a UV glue coated glass slide, UV glue was dropped cast on microscopy glass slide and cured to create a thin film of UV glue. Both UV glue channel and UV glue coated glass slide were plasma treated for 1 min, pressed together and UV cured. Tygon tubing were inserted into the inlet/outlet holes and sealed with UV glue.

Device Operation: PDMS channels and three-way valve (Masterflex polycarbonate three-way stopcock valve, Cole-Parmer Inc., Vernon Hills, IL, USA) were pre-filled with 70% ethanol before connecting to resin packed μ SEC device. Two separate syringe pumps (CX Fusion 200, Chemyx Inc., Stafford, TX, USA) were used to perfuse sample and sheath flows (PBS) into μ SEC device. To minimize EVs' adhesion on the channel wall, the μ SEC channel was perfused with 1% bovine serum albumin (BSA) at 10 μ L min⁻¹ for 30 min before washing with filtered PBS at 10 μ L min⁻¹ for 1 h to flush away remaining BSA. Sheath flow rate was adjusted until center channel flow rate was between 1.5 to 1.6 μ L min⁻¹ by measuring the volume output at outlet 4. Sample flow and sheath flow were set to 5 and 50 μ L min⁻¹ respectively. During plug generation, the valve was switched from outlet 2 to outlet 3 for 30–60 s. After sample injection, sample flow was stopped, and the valve was switched back to outlet 2. Sheath flow was readjusted to previous optimized flow rate to start elution. Each SEC fraction was collected for 200 s. The device was mounted on a Nikon Eclipse Ti inverted phase-contrast microscope (Nikon Instruments Inc., Melville, NY, USA) equipped with Metamorph software (WSN-META-MMACQMIC, Molecular Devices, Sunnyvale, CA, USA) for quantifying fluorescent intensity in the detection channel using fluorescence microscopy.

Study Approval: Written informed consent was obtained from all subjects during recruitment for this study. 2 mL whole blood samples collected from venipuncture into sodium citrate vacutainers (BD Biosciences, Franklin Lakes, NJ, USA), and protocols were approved by the institutional review boards (IRB) of Nanyang Technological University (IRB-2021-01-037).

Supporting Information

Supporting Information is available from the Wiley Online Library or from the author.

Acknowledgements

H.W.H., S.Y.L., H.B.O., H.M.T., L.G., F.K., M.U., R.D., and M.D. conceived the idea and designed the experiments. S.Y.L., H.B.O., H.M.T., L.G. performed the experiments and analyzed the data. F.K., M.U. assisted in Western blot analysis and TEM. R.D. and M.D. assisted in subject recruitment and data analysis. S.Y.L. and H.W.H. wrote the manuscript. All authors reviewed the manuscript. H.W.H. would like to acknowledge the kind financial support from SMART Innovation Centre (ING-000539 BIO IGN and ING-001058 BIO IGN), and NTU Startup grant. S.Y.L. and L.G. would like to acknowledge support from the NTU Research Scholarship. The authors would like to acknowledge Biorender.com for figures creation.

Conflict of Interest

The authors declare no conflict of interest.

Data Availability Statement

The data that support the findings of this study are available from the corresponding author upon reasonable request.

Keywords

blood, extracellular vesicles, microfluidic, miniaturization, size exclusion chromatography

Received: July 28, 2021

Revised: December 2, 2021

Published online:

- [1] J. Tian, G. Casella, Y. Zhang, A. Rostami, X. Li, *Int. J. Biol. Sci.* **2020**, *16*, 620.
- [2] M. Monguió-Tortajada, C. Gálvez-Montón, A. Bayes-Genis, S. Roura, F. E. Borràs, *Cell. Mol. Life Sci.* **2019**, *76*, 2369.
- [3] H. Yan, Y. Li, S. Cheng, Y. Zeng, *Anal. Chem.* **2021**, *93*, 10343.
- [4] Y. Lu, D. Liu, Q. Feng, Z. Liu, *Front. Immunol.* **2020**, *11*, 943.
- [5] N. Noren Hooten, M. K. Evans, *Am. J. Physiol.: Cell Physiol.* **2020**, *318*, C1189.
- [6] A. Möller, R. J. Lobb, *Nat. Rev. Cancer* **2020**, *20*, 697.
- [7] M. Mathieu, L. Martin-Jaular, G. Lavie, C. Théry, *Nat. Cell Biol.* **2019**, *21*, 9.
- [8] B. Pang, Y. Zhu, J. Ni, J. Thompson, D. Malouf, J. Bucci, P. Graham, Y. Li, *Theranostics* **2020**, *10*, 2309.
- [9] V. Agrahari, V. Agrahari, P.-A. Burnouf, C. H. Chew, T. Burnouf, *Trends Biotechnol.* **2019**, *37*, 707.
- [10] A. Shehzad, S. U. Islam, R. Shahzad, S. Khan, Y. S. Lee, *Pharmacol. Ther.* **2021**, *223*, 107806.
- [11] R. C. de Abreu, H. Fernandes, P. A. da Costa Martins, S. Sahoo, C. Emanueli, L. Ferreira, *Nat. Rev. Cardiol.* **2020**, *17*, 685.
- [12] R. E. Lane, D. Korbie, M. Trau, M. M. Hill, *Proteomics* **2019**, *19*, 1800156.
- [13] K. Takov, D. M. Yellon, S. M. Davidson, *J. Extracell. Vesicles* **2019**, *8*, 1560809.
- [14] K. Brennan, K. Martin, S. FitzGerald, J. O'Sullivan, Y. Wu, A. Blanco, C. Richardson, M. Mc Gee, *Sci. Rep.* **2020**, *10*, 1039.
- [15] K. Sidhom, P. O. Obi, A. Saleem, *Int. J. Mol. Sci.* **2020**, *21*, 6466.
- [16] M. Morozumi, H. Izumi, T. Shimizu, Y. Takeda, *J. Dairy Sci.* **2021**, *104*, 6463.
- [17] S. Gandham, X. Su, J. Wood, A. L. Nocera, S. C. Alli, L. Milane, A. Zimmerman, M. Amiji, A. R. Ivanov, *Trends Biotechnol.* **2020**, *38*, 1066.
- [18] Y. Gu, C. Chen, Z. Mao, H. Bachman, R. Becker, J. Rufo, Z. Wang, P. Zhang, J. Mai, S. Yang, *Sci. Adv.* **2021**, *7*, eabc0467.
- [19] M. Wu, Y. Ouyang, Z. Wang, R. Zhang, P.-H. Huang, C. Chen, H. Li, P. Li, D. Quinn, M. Dao, *Proc. Natl. Acad. Sci. USA* **2017**, *114*, 10584.
- [20] H. M. Tay, S. Y. Leong, X. Xu, F. Kong, M. Upadya, R. Dalan, C. Y. Tay, M. Dao, S. Suresh, H. W. Hou, *Lab Chip* **2021**, *21*, 2511.
- [21] H.-K. Woo, V. Sunkara, J. Park, T.-H. Kim, J.-R. Han, C.-J. Kim, H.-I. Choi, Y.-K. Kim, Y.-K. Cho, *ACS Nano* **2017**, *11*, 1360.
- [22] E. V. S. Maciel, A. L. de Toffoli, E. Sobieski, C. E. D. Nazário, F. M. Lanças, *Anal. Chim. Acta* **2020**, *1103*, 11.
- [23] X. Xie, L. T. Tolley, T. X. Truong, H. D. Tolley, P. B. Farnsworth, M. L. Lee, *J. Chromatogr. A* **2017**, *1523*, 242.
- [24] Y. Li, M. Dvořák, P. N. Nesterenko, R. Stanley, N. Nuchtavorn, L. K. Krčmová, J. Aufartová, M. Macka, *Anal. Chim. Acta* **2015**, *896*, 166.
- [25] D. Kitka, J. Mihály, J.-L. Fraikin, T. Beke-Somfai, Z. Varga, *Sci. Rep.* **2019**, *9*, 19868.
- [26] D. A. V. Medina, E. V. S. Maciel, F. M. Lanças, *TrAC, Trends Anal. Chem.* **2020**, *131*, 116003.
- [27] F. Haghghi, Z. Talebpour, A. S. Nezhad, *TrAC, Trends Anal. Chem.* **2018**, *105*, 302.
- [28] H. Yin, K. Killeen, *J. Sep. Sci.* **2007**, *30*, 1427.
- [29] H. Yin, K. Killeen, R. Brennen, D. Sobek, M. Werlich, T. van de Goor, *Anal. Chem.* **2005**, *77*, 527.
- [30] S. C. Jacobson, R. Hergenroder, L. B. Koutny, R. Warmack, J. M. Ramsey, *Anal. Chem.* **1994**, *66*, 1107.
- [31] S. C. Jacobson, L. B. Koutny, R. Hergenroder, A. W. Moore, J. M. Ramsey, *Anal. Chem.* **1994**, *66*, 3472.
- [32] X. Bai, H. J. Lee, J. S. Rossier, F. Reymond, H. Schafer, M. Wossner, H. H. Girault, *Lab Chip* **2002**, *2*, 45.
- [33] Z. Wang, W. Wang, G. Chen, W. Wang, F. Fu, *J. Sep. Sci.* **2010**, *33*, 2568.
- [34] A. Nagy, A. Gaspar, *J. Chromatogr. A* **2013**, *1304*, 251.
- [35] S. Kabiri, M. D. Kurkuri, T. Kumeria, D. Losic, *RSC Adv.* **2014**, *4*, 15276.
- [36] A. Gaspar, M. E. Piyasena, F. A. Gomez, *Anal. Chem.* **2007**, *79*, 7906.
- [37] X. Illa, W. De Malsche, J. Bomer, H. Gardeniers, J. Eijkel, J. R. Morante, A. Romano-Rodríguez, G. Desmet, *Lab Chip* **2009**, *9*, 1511.
- [38] A. A. Soukas, H. Hao, L. Wu, *Trends Endocrinol. Metab.* **2019**, *30*, 745.
- [39] D. Sticker, R. Geczy, U. O. Hafeli, J. P. Kutter, *ACS Appl. Mater. Interfaces* **2020**, *12*, 10080.
- [40] R. R. Svejidal, D. Sticker, C. Sønderby, J. P. Kutter, K. D. Rand, *Anal. Chim. Acta* **2020**, *1140*, 168.
- [41] P. Wägli, B. Guélat, A. Homsy, N. De Rooij, *Proc. of the 14th Int. Conf. on Miniaturized Systems for Chemistry, Life Sciences, Chemical and Biological Microsystems Society (CBMS)*, Groningen, The Netherlands **2010**, pp. 3–7.
- [42] Y. Markovitz-Bishitz, Y. Tauber, E. Afrimzon, N. Zurgil, M. Sobolev, Y. Shafran, A. Deutsch, S. Howitz, M. Deutsch, *Biomaterials* **2010**, *31*, 8436.
- [43] D. Bartolo, G. Degré, P. Nghe, V. Studer, *Lab Chip* **2008**, *8*, 274.
- [44] K. Takov, D. M. Yellon, S. M. Davidson, *J. Extracell. Vesicles* **2017**, *6*, 1388731.
- [45] S. Stremersch, T. Brans, K. Braeckmans, S. De Smedt, K. Raemdonck, *Int. J. Pharm.* **2018**, *548*, 783.
- [46] A. Morales-Kastresana, B. Telford, T. A. Musich, K. McKinnon, C. Clayborne, Z. Braig, A. Rosner, T. Demberg, D. C. Watson, T. S. Karpova, *Sci. Rep.* **2017**, *7*, 1878.
- [47] E. J. Van Der Vlist, E. N. Nolte, W. Stoorvogel, G. J. Arkesteijn, M. H. Wauben, *Nat. Protoc.* **2012**, *7*, 1311.
- [48] E. Sollier, C. Murray, P. Maoddi, D. Di Carlo, *Lab Chip* **2011**, *11*, 3752.
- [49] K. Lee, K. Fraser, B. Ghaddar, K. Yang, E. Kim, L. Balaj, E. A. Chiocca, X. O. Breakefield, H. Lee, R. Weissleder, *ACS Nano* **2018**, *12*, 494.
- [50] P. Zhang, X. Zhou, M. He, Y. Shang, A. L. Tetlow, A. K. Godwin, Y. Zeng, *Nat. Biomed. Eng.* **2019**, *3*, 438.
- [51] C. Z. Lim, Y. Zhang, Y. Chen, H. Zhao, M. C. Stephenson, N. R. Ho, Y. Chen, J. Chung, A. Reilhac, T. P. Loh, *Nat. Commun.* **2019**, *10*, 1144.